

Role of Cellulose Nanocrystals on the Microstructure of Maleic Anhydride Plasma Polymer Thin Films

Michel M. Brioude,^{†,‡} Vincent Roucoules,[§] Hamidou Haidara,[§] Laurent Vonna,[§]
and Marie-Pierre Laborie^{*,†,‡}

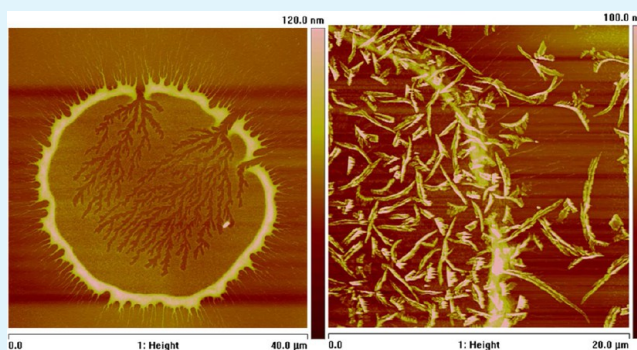
[†]Chair of Forest Biomaterials, Faculty of Environment and Natural Resources, University of Freiburg, Werthmannstrasse 6, Freiburg 79098, Germany

[‡]Freiburg Materials Research Center (FMF), University of Freiburg, Stefan-Meier-Strasse 21, Freiburg 79104, Germany

[§]Institut de Science de Matériaux de Mulhouse CNRS UMR7361, Université de Haute-Alsace, 15 rue Jean Starcky, PB 2488, Mulhouse Cedex 68057, France

ABSTRACT: Recently, it was shown that the microstructure of a maleic anhydride plasma polymer (MAPP) could be tailored *ab initio* by adjusting the plasma process parameters. In this work, we aim to investigate the ability of cellulose nanocrystals (CNCs) to induce topographical structuration. Thus, a new approach was designed based on the deposition of MAPP on CNCs model surfaces. The nanocellulosic surfaces were produced by spin-coating the CNC suspension on a silicon wafer substrate and on a hydrophobic silicon wafer substrate patterned with circular hydrophilic micro-sized domains (diameter of $86.9 \pm 4.9 \mu\text{m}$), resulting in different degrees of CNC aggregation. By depositing the MAPP over these surfaces, it was possible to observe that the surface fraction of nanostructures increased from 20% to 35%. This observation suggests that CNCs can act as nucleation points resulting in more structures, although a critical density of the CNCs is required.

KEYWORDS: maleic anhydride, plasma polymerization, cellulose nanocrystals, patterned surface, spin-coating



INTRODUCTION

Surface modification of materials is a potent approach to control the chemistry and the topography of surfaces, thereby providing a mean to tailor adhesion properties, biological activity, surface transport properties, and so forth.¹ Among the surface modification techniques, plasma polymerization stands out as a solvent-free and versatile process able to produce ultrathin and pinhole-free polymer-like layers² from almost any organic vapor on any substrate without the need for pretreatment.^{3,4} By adjusting the conditions of plasma deposition and the selection of the monomer, it is possible to control not only the chemistry but also the morphology of the coating. For example, fluorocarbon plasma exhibits different morphologies (ribbons, petals, domes, and dots) depending on the conditions applied.^{5–11} Likewise, different nanoscale morphologies have been recently reported in a maleic anhydride plasma polymer (MAPP) prepared through pulsed excitation.^{12,13} Beads, branched, and needlelike complex nanostructures were for the first time observed in this system and found to depend on plasma parameters, namely, peak power, duty cycle, frequency, and time.^{12,13} The possibility to tune MAPP morphology beside the well-established tunability of MAPP chemistry^{22–25} further increases the attractivity of

MAPPs for various applications^{14–16} and particularly as platforms for biosurface engineering.^{17–21}

Nanoparticles exhibit remarkable effect on polymer morphology and especially on polymer crystallization kinetics.²⁶ When dealing with polymer thin films, nanoparticles can also affect the film stability.^{27,28} In both cases, nanoparticles act as nucleating agents contributing to crystallization or destabilizing the polymer film. Cellulose nanocrystals (CNCs) are rodlike nanoparticles most commonly produced by acid-catalyzed hydrolysis of cellulose amorphous domains. Because of their biodegradability, low density, high mechanical strength, and stiffness, CNCs are valuable nanoscale reinforcements for composites; in such nanocomposites, the role of CNCs as nucleation agents to control polymer crystallization has been repeatedly demonstrated.^{31–36} Additionally, the codeposition of MA and CNCs in a pulsed plasma reactor was recently reported to generate a microstructuration of MAPP thin films.¹ This microstructuration was ascribed to CNC-destabilizing action and buckling of metastable MAPP thin films.^{1,37}

Received: April 16, 2015

Accepted: June 2, 2015

Published: June 2, 2015

The possibility of using the CNCs for inducing topographical microscale and nanoscale structuration of thin films can open new opportunities for these biobased nanoparticles and unique properties for the resulting nanocomposite thin films; however, tailor-designing the micro- and nanoscale structure of such nanocomposite films is only possible if one understands the mechanism of CNC-induced structuration on MAPPs. The current evidence of nanostructure formations in MAPPs and microstructuration in CNC/MAPP nanocomposites raise the question of the possible role of the CNCs. Are CNCs catalyzing the formation of complex structures in MAPP films^{12,13} or are CNCs simply destabilizing the MAPP films?^{1,37}

To answer this question, the deposition of CNCs on the substrate prior to MAPP deposition is an interesting idea, since it enables controlling not only the amount of CNCs but also their distribution on the substrate. Since CNCs form stable suspensions in water, spin-coating is a simple way to produce nanocellulosic model surfaces. Kontturi et al. successfully deposited well-dispersed submonolayer of CNCs using spin-coating.³⁸ Besides, a heterogeneous and patterned distribution of CNCs could be achieved by modifying the substrate with hydrophilic/hydrophobic domains such that CNCs would preferentially deposit on the hydrophilic domains during the wetting/dewetting process of a CNC dispersion.³⁹

In this paper, we propose the preparation of nanocellulosic surfaces with different patterns, namely, homogeneously dispersed CNCs and locally concentrated CNCs, followed by the deposition of MAPPs under different conditions. By doing so, the role of CNCs on the microstructuration of MAPP films can be revealed as a function of CNC distribution on the substrate; either CNCs act as nucleation points inducing the formation of structures or they locally destabilize the film resulting in wrinkled surfaces.

■ EXPERIMENTAL SECTION

Preparation and Morphological/Surface Characterization of CNCs. CNCs were produced via acid hydrolysis of microcrystalline cellulose (MCC; AVICEL PH-101, Fluka) in 63.5% (w/w) sulfuric acid at 44 °C for 2 h, according to the procedure reported by Bondeson et al.⁴⁰ After hydrolysis, the suspension was washed with deionized water using repeated centrifuge cycles to remove the excess of sulfuric acid and the remaining microfibrils. The CNCs obtained from centrifugation were then concentrated and washed using dialysis with deionized water for 3 weeks and stored in a refrigerator. The calculated yield for the whole process was around 40%. All the experiments were performed with CNC suspensions at 0.05 wt %. Before use, the suspensions were sonicated to redisperse the CNCs.

The length and width of the CNCs were estimated from atomic force microscopy (AFM) images using nanoscope software. The length was obtained by direct measurement, and the width was measured from the height profile of single nanocrystals to avoid the broadening effect intrinsic from AFM analysis. The crystallinity of the CNCs was determined by X-ray diffraction in transmission mode on a diffractometer STOE (Darmstadt, Germany, STADI-P) using Cu K α as the radiation ($\lambda = 1.54 \text{ \AA}$) at 40 kV and 30 mA. The data was acquired in a 2θ range between 3° and 70° with a 0.02° resolution. The crystallinity index (CrI) was determined via the method described by Segal et al.⁴¹ The CNC sulfur content was assessed by conductometric titration according to a method described elsewhere^{42,43} and used to assess the degree of substitution (DS) of anionic sulfate ester groups, which are introduced during the hydrolysis with sulfuric acid.^{29,30}

Preparation of Model Nanocellulosic Surfaces by Spin-Coating. The procedure used to obtain the nanocomposites consisted in the preparation of model nanocellulosic surfaces followed by the MA plasma deposition. In order to prepare the nanocellulosic surfaces,

the CNCs were deposited onto single-side-polished silicon wafers cut in approximately $1 \times 1 \text{ cm}^2$ pieces and cleaned with piranha solution (1:3 v/v mixture of 30% H₂O₂ and 98% H₂SO₄) for 30 min to remove organic contaminants and create a hydroxyl-rich surface.⁴⁴ The substrate was completely covered by drops of the CNCs suspension in order to produce surfaces with homogeneous CNC dispersion along the whole substrate (center and border) and spin-coated at a speed of 4000 rpm for 30 s (initial acceleration was 2000 rpm s⁻¹). The effect of exposing the nanocellulosic surfaces to a vacuum inside the reactor was evaluated by placing the samples for 5 min at the same position used for MAPP deposition.

Before plasma deposition, the distribution of the CNCs onto the substrate was observed by AFM. At least three different positions were checked to confirm that the distribution of CNCs was homogeneous, that is, that the CNC surface fractions were similar. The CNC surface coverage was estimated by treating the AFM images with the software ImageJ.

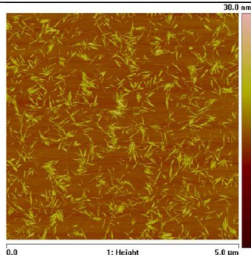
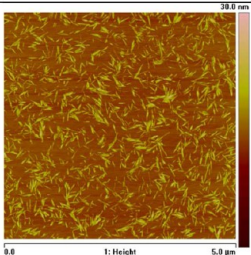
Spin-coating of the CNC suspension on a hydrophobic silicon wafer substrate patterned with circular hydrophilic microsized domains was also tested. The patterned surface was obtained in a two-stage process: (1) formation of a hydrophobic self-assembled monolayer (SAM) on the hydrophilic silicon wafer and (2) local etching of the SAM by UV exposure creating the circular hydrophilic domains. In order to produce the hydrophobic SAM, the silicon wafer was previously cleaned in piranha solution, rinsed with deionized water, and blown dry under a stream of nitrogen. This cleaned and hydroxylated silicon wafer was then immersed in a 2 mM solution of hexadecyltrichlorosilane in cyclohexane for 12 h (overnight). After the completion of the adsorption and grafting step, the sample was removed from the solution and sonicated in cyclohexane for 10 min. This last operation aimed at desorbing any excess aggregate or molecule physisorbed onto the surface.⁴⁴ With the completion of this step, a chromium/quartz mask composed of chromium-free hexagons with a distance between parallel sides of 64 μm was placed on top of the hydrophobic SAM and then exposed to UV light for 10 h.

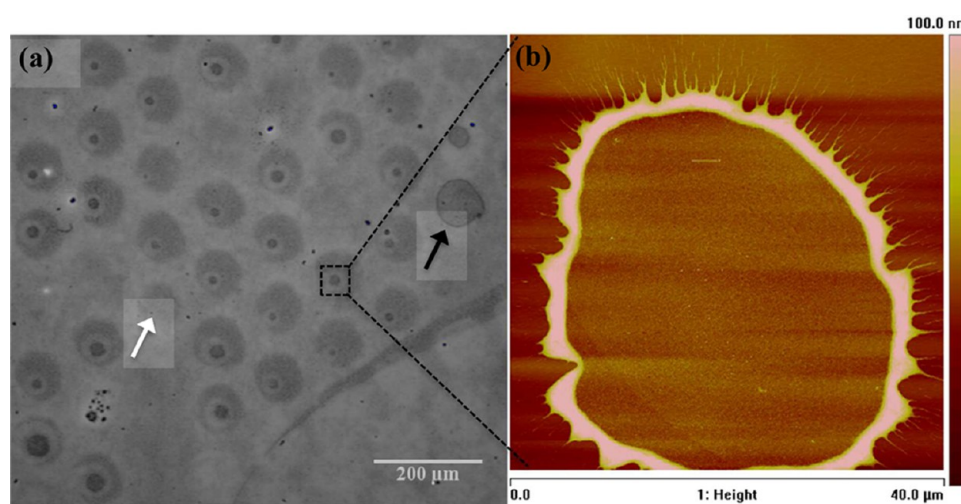
Deposition of MAPPs on Nanocellulosic Surfaces. MA monomer powder (Prolabo 99.5% purity, used as received) was grounded into a fine powder and loaded into a stoppered glass gas delivery tube. The experiments were conducted in an electrode-less cylindrical glass reactor enclosed in a Faraday cage, as described elsewhere.²⁴ The reactor chamber was connected to a MA monomer gas inlet on one side and to a Pirani pressure gauge on the other side, in series with a two-stage rotary pump connected to a liquid nitrogen cold trap. The nanocellulosic surfaces were placed onto a glass support and centered along the externally wound copper coil (16 cm from the gas inlet). The substrates were placed precisely between the first and second copper coils, since at this position, the plasma excitation is more homogeneous, producing more reproducible results. The latter was connected to an L-C matching network and a radio frequency generator providing an output frequency of 13.56 MHz. The shape of the electrical pulses was monitored with an oscilloscope, and the average power (P) delivered to the system was calculated according to eq 1, where P_p is the average continuous wave power output (i.e., peak power), DC is the duty cycle, t_{on} is the pulse-on time, and t_{off} is the pulse-off time:

$$P = P_p \cdot \text{DC} = P_p \cdot \frac{t_{\text{on}}}{t_{\text{on}} + t_{\text{off}}} \quad (1)$$

Before each experiment, the reactor was cleaned for 30 min with a high-power air plasma ($P = 60 \text{ W}$) treatment. The MA vapor was introduced into the reactor by sublimation under evacuation at a constant reactor pressure of 0.2 mbar and a constant flow rate of approximately 0.03 sccm. The plasma was initiated through a high-frequency generator at different conditions of P_p , DC, and frequency ($1/(t_{\text{on}} + t_{\text{off}})$). The samples were named according to the condition of plasma deposition in the following order: " $P_p/\text{DC}/\text{frequency}$ " or " P_p/CW " for pulsed or continuous wave deposition, respectively. The time of deposition was 20 min for all the samples. Upon completion of the deposition, the radio frequency generator was switched off while the

Table 1. Morphology and Surface Fraction of the Nanocellulosic Surfaces Deposited on a Piranha-Treated Silicon Wafer after Spin-Coating and after Vacuum Exposure

	After Spin-Coating	After Vacuum
Morphology		
Center Surface Fraction	20.4 ± 2.1 %	27.2 ± 5.3 %
Border Surface Fraction	19.6 ± 2.3 %	27.9 ± 8.2 %
Average Surface Fraction	20.0 ± 2.1 %	27.7 ± 6.7 %

**Figure 1.** (a) Optical microscopy of the hydrophobic silicon wafer containing circular hydrophilic pattern microdomains. (b) Height AFM image of the darker spots inside the hydrophilic domains.

monomer continued to flow for about 2 min prior to venting to atmospheric pressure and unloading the samples. This step prevents the reaction of residual free radicals in the plasma polymer thin film with undesirable atmospheric atoms.

Characterization. AFM. The morphology of the nanocellulosic and MAPP films was analyzed by AFM using a Dimension 3000 scanning probe microscope (Digital Instrument), running with a Nanoscope IIIA controller (Digital Instrument) and operating in tapping mode. Silicon cantilevers with a spring constant of 20–100 N m⁻¹ were used for the measurements. The surface fraction of the CNCs and MAPP structures were calculated through the treatment of the height AFM images with the software ImageJ by application of a binarization and thresholding procedure, followed by the calculation of the total surface area and the surface area of the structures (black areas).

RESULTS

Characterization of CNCs and Nanocellulosic Model Surfaces. The CNCs obtained by the hydrolysis reaction of MCC exhibited an average length and width of 206 ± 53 nm and 5 ± 1 nm, respectively. These dimensions are comparable to the results reported by Bondeson et al. in which the length was found to be between 200 and 400 nm while the width was smaller than 10 nm.⁴⁰ The estimated CrI of the CNCs was 81%. The obtained result is in the same range of CrI registered

for CNCs prepared under the same conditions, in which the value ranged from 75% to 85%.^{45,46} The sulfur content on the CNC surface is an important factor for the stability of the colloidal suspension. The value obtained via conductometric titration was 0.95 ± 0.01% and corresponded to a DS of 0.048. Sulfur contents ranging from 0.5% to 1.0% were found by different authors.^{42,43,47}

The nanocellulosic model surfaces obtained by spin-coating a 0.05 wt % CNC suspension on a piranha-treated silicon wafer resulted in the formation of a noncontinuous film, showing regions of isolated and agglomerated CNCs (clusters). These agglomerations form large clusters in rare cases, despite the sonication of the suspension before application, disturbing the homogeneity of the surfaces (data not shown). To ensure the reproducibility of the results, the substrate was fully covered by the suspension before spin-coating, and the morphology of the model surface was checked by AFM in several regions near the center and the borders. A possible effect of a vacuum on the distribution of the CNCs was also assessed, since the surface is exposed to a pressure of ~10⁻³ mbar inside the reactor, prior to the plasma polymerization. No differences in the surface fraction were observed between the center and the border, and the exposure to a vacuum did not affect the dispersion of the CNCs (Table 1). Since different areas were analyzed before and

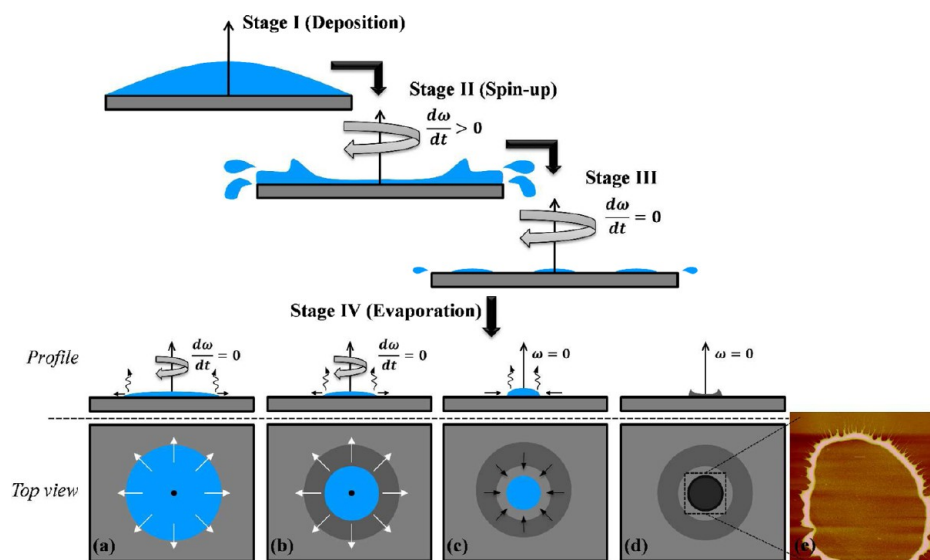


Figure 2. Scheme highlighting the main steps of the spin-coating process (deposition, spin-up, stable fluid outflow, and evaporation). The evaporation step is depicted in detail. (a) Beginning of evaporation overlapping stage three. The fluid spreads and covers completely the hydrophilic domain, forced by the centrifugal force. (b) The evaporation of the water causes a slow receding of the contact line during stage III and spin-off. (c) By the stop of spinning, the water drop relaxes resulting in a fast inward movement, which collects the cellulose nanocrystals. (d, e) the collection of the CNCs generates an increase of viscosity in the receding front, causing its deceleration. Fingering in a final stage is due to the destabilization of the contact line caused by the presence of the nanoparticles.

after vacuum exposure, small differences in the surface fraction were expected.

Spin-coating the CNC suspension on the hydrophobic substrate within circular hydrophilic patterns resulted in the formation of three different discernible areas: a hydrophobic area (light gray), hydrophilic circular microdomains (gray area), and a smaller circular area (dark gray) inside the hydrophilic domain (Figure 1a). A close view of the darker spots revealed a high density of CNCs confined on these areas, which can be referred to as CNC islands (Figure 1b). The hydrophilic domains exhibited a homogeneous size distribution while the CNC islands (dark inner spots) were very heterogeneous in size going from none (white arrow in Figure 1a) to the entire covering of the whole hydrophilic domain (black arrow in Figure 1a). The estimated diameters of the hydrophilic domains and the CNC islands are 86.9 ± 4.9 and 23.2 ± 13.9 μm , respectively. The CNC islands exhibited an accumulation of CNCs on the border (Figure 1b). Despite the similarity with the coffee-ring morphology, this pattern was formed due to the evaporation and relaxation of a remaining drop confined on the hydrophilic domain with the completion of the spin-coating process. The outer region of the hydrophilic circular domains (light gray area) surrounding the dark CNCs islands might represent the action of the water drop relaxation, which leads to the collection of the CNCs and their accumulation in the border of the darker spot, as well as the formation of the fingers as shown in Figure 1b.

In order to understand and support the hypothesis for the CNC island formation, a complete description of the spin-coating process is needed. According to Sahu et al, the spin-coating process can be divided into four stages: (I) deposition, (II) spin-up, (III) stable fluid outflow, and (IV) evaporation (Figure 2).⁴⁸

The deposition was made on a stationary substrate by covering its whole area with the CNC suspension. The spin-up stage starts when the substrate is accelerated up to the final rotational speed. During this stage, the water is aggressively

expelled from the substrate by rotational motion. By reaching the desired rotational speed, a noncontinuous layer of fluid is expected for this system, since the water easily slides over the hydrophobic areas but remains on the hydrophilic circular domains. The confined fluid layers are thin enough so that the resisting (sticking) viscous shear overcomes the rotation-induced drag.⁴⁹ At this point, it is possible to idealize this system as a process in which several microdrops of CNC suspension (confined in the hydrophilic domain) are submitted to spin-coating.

The following stages are the most important for the final morphology of the deposited coating. The third stage is characterized by a constant rotational speed (ω) and a prevalence of the fluid viscous shear force (sticking) given by \mathcal{F}_η (eq 2) over their thinning behavior:

$$\mathcal{F}_\eta = \left(\frac{\eta_{\text{drop}} \cdot r \cdot \omega}{h_{\text{drop}}} \right) \cdot A_{\text{spot}} \quad (2)$$

where η is the viscosity of the drop, r is the radius measured from the center of the substrate to the center of the drop, h is the thickness of the drop, and A is the spot area.

At this stage, a thin layer of fluid is forced to spread over the hydrophilic domain by the centrifugal force (\mathcal{F}_c) given by eq 3:

$$\mathcal{F}_c \sim (\rho V)_{\text{drop}} \cdot r \cdot \omega^2 \quad (3)$$

where ρ and V are the density and the volume of the fluid, respectively.

Overlapping the third stage, the evaporation of the drops starts to take place with the movement of the contact line and reduction of the wetted area (Figure 2a, b). With the completion of the spin-coating process, the action of the centrifugal force on the remaining drops decreases regularly to cease, causing their instantaneous relaxation. This relaxation results in a very fast inward radial movement of the contact line to accommodate the contact area and the angle of the residual

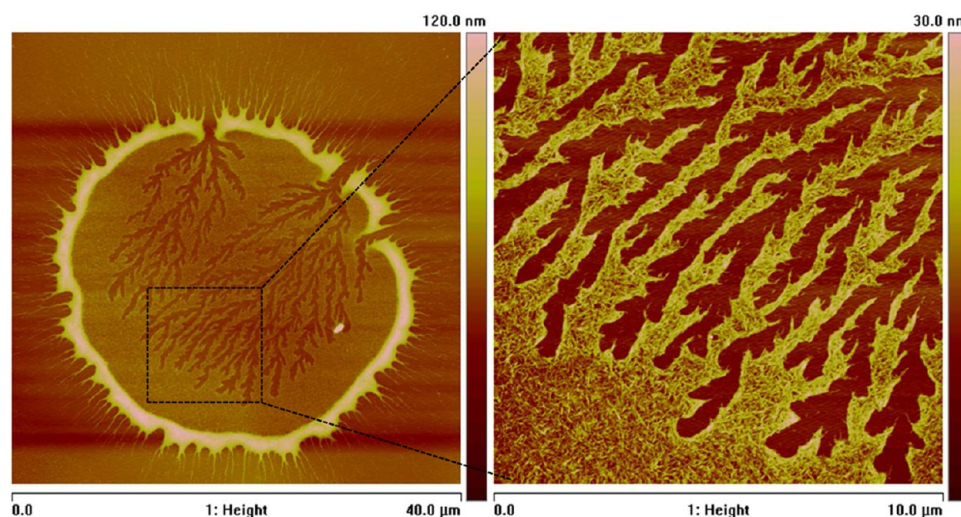


Figure 3. Formation of arborescent pattern in CNC high-density domain.

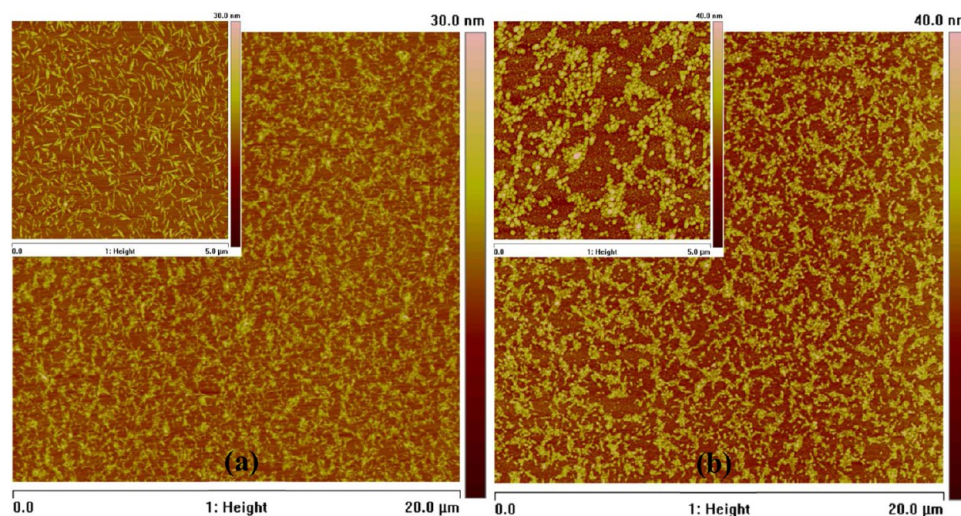


Figure 4. Height AFM images of samples (a) 10/2/816 and (b) 20/CW.

drop to their “equilibrium” values. The high velocity of the receding front together with the high viscosity of the suspension produces a very high shear stress, which drags and collects the CNCs (Figure 2c). On the other hand, the collection of the CNCs causes at the same time their accumulation and a significant increase of viscosity in the receding front. These combined effects cause the deceleration of the receding front and in a final stage the formation of fingers as a result of the destabilization of the contact line by the nanoparticles (Figure 2d, e).

The front instability during the drying process of the nanoparticles suspension is known, and different parameters affect the fingering formation such as chemical potential, particle mobility, and particle–particle interactions.⁵⁰ Although the hypothesis for the final pattern is not strictly drying-induced but more relaxation-induced, Crivoi and Duan obtained a similar drying pattern when the mobility of the particle is high and the particle–particle interaction is low.⁵¹ In this case, only the transport properties play a role, since the mobile and individual particles are more easily collected by the drying front and pulled inward. In our case, this collection leads to the formation of a thick peripheral ring, which slows down the retraction of the contact line, pinning definitively the tiny

residual drop (Figure 2e). These observations support the hypothesis of low particle–particle interaction, and the presence of the anionic sulfate ester groups on the CNCs contribute to their mutual repulsion.

In addition, the low particle–particle and particle–substrate interactions usually lead to complete collection of the particles within the receding drop in a final thick and featureless aggregate.⁴⁹ In this study, it resulted in the formation of the arborescent pattern observed in Figure 3.

This section focused mainly on the CNC islands, since CNC density is an important aspect for understanding the role of the CNCs on the structure formation during the MAPP deposition or in the destabilization of the film. Further optimization in the development of the chemical patterned substrate or increasing the concentration of the CNC suspension might result in a homogeneous patterned surface with the CNCs covering completely and uniformly the hydrophilic domains.

Morphology of the MAPP/CNC Nanocomposite Films.

The main hypothesis for the formation of the structures in the MAPP during pulsed excitation relies on the diffusion of the radicals during the pulse-off time and further reaction with nucleation points that arise from a local surface excitation of the substrate during the pulse-on time.¹² These excited surface

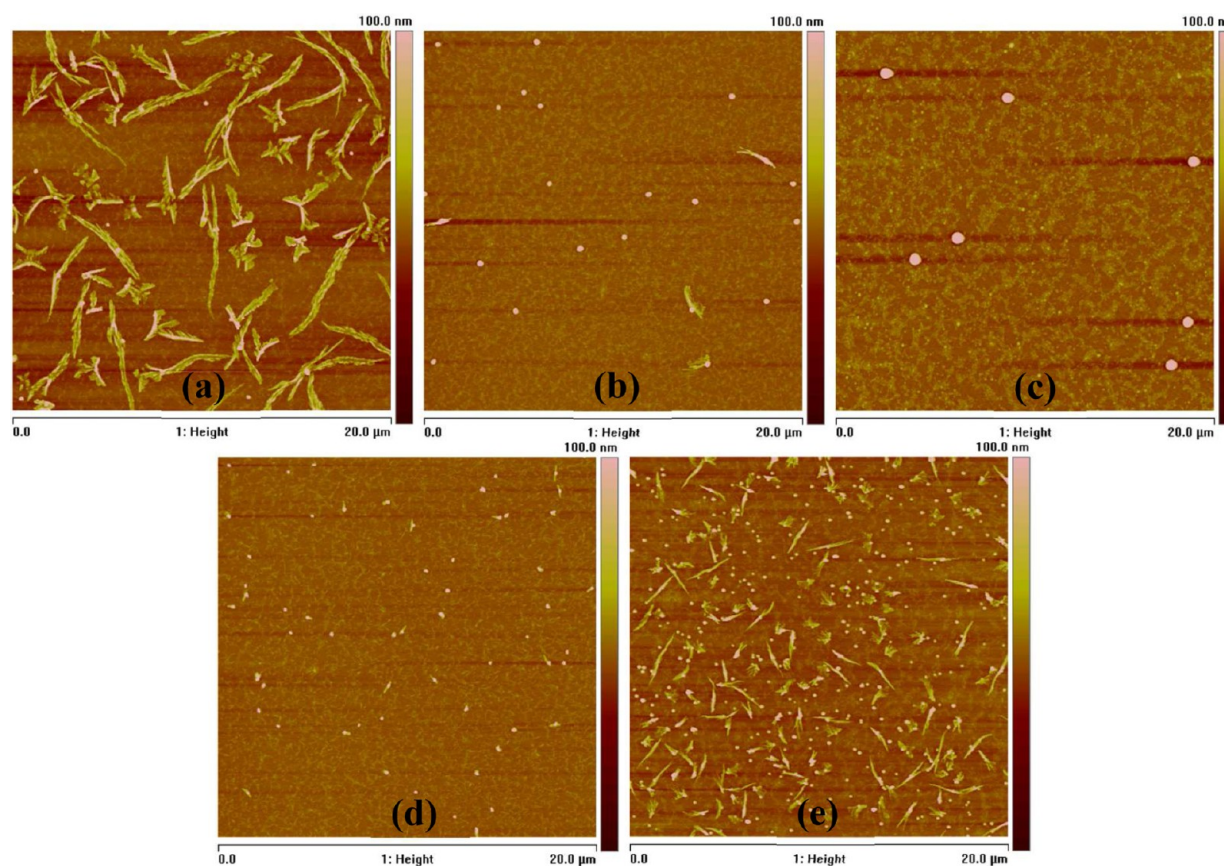


Figure 5. Height AFM images of MA/CNC films exhibiting the formation of the structures and the effect of plasma parameters (power, DC, and frequency) in samples (a) 20/2/204, (b) 20/10/204, (c) 20/50/204, (d) 20/2/1633, and (e) 50/2/204.

points are formed mainly in the early stage of the plasma deposition and result initially in the formation of spherical structures called beads that are further converted into the complex structures (needlelike and branched) with the continued reaction between radicals and beads.¹³ In addition, two requirements should be fulfilled in order to develop these MAPP structures: a pulse-off time provided by the pulsed excitation, which allows the diffusion of the radicals on the surface, and enough power to excite the substrate and create the nucleation points.¹² Therefore, the presence of the CNCs homogeneously distributed or as highly concentrated CNC islands (patterned surface) was expected to induce two possible effects: (1) provide more nucleation sites resulting in an increased amount of structures or (2) destabilize the MAPP coating resulting in a completely wrinkled surface, as observed by Samyn et al.³⁷

By depositing the MAPP on the homogeneously distributed CNCs under conditions in which the formation of the structures was not expected, such as 10/2/816 (very low power and DC) and 20/CW (continuous wave), the morphologies exhibited in Figure 4 were obtained. In both cases, the nonformation of the structures was confirmed, suggesting a behavior similar to that previously observed when depositing MAPP films on neat, CNC-free wafers.¹² In addition, the individual or clustered CNCs were still clearly observed in sample 10/2/816 where the thickness of the coating is thinner than 10 nm but also for sample 20/CW that is more than 200 nm thicker. The surface roughness estimated from the root mean squared roughness (R_q) increased in comparison with the neat MAPP films from 0.39 to 2.24 nm

and from 2.66 to 5.12 nm for samples 10/2/816 and 20/CW, respectively.

The MAPP deposition under conditions in which the structures were previously observed on neat wafers could show the influence of the dispersed CNCs on the formation of the structures. According to Brioude et al, longer structures were obtained for sample 20/2/204 on neat wafers, which provided enough power to produce MA radicals and create some nucleation points by local excitation of the substrate and long pulse-off time (ca. 4800 μ s) for the radicals migration and reaction with the nucleation points.¹² Figure 5a shows the morphology of sample 20/2/204 deposited on the nanocellulosic surface. Likewise, very long needlelike and branched structures were observed together with few beads.

The increase of the DC to 10% (Figure 5b) greatly reduced the length and the density of the complex structures but increased the number of the beads. Further increase of DC to 50% resulted only in the formation of beads (Figure 5c).

Increasing the frequency and keeping the other parameters constant (sample 20/2/1633, Figure 5d) resulted in the formation of beads and very short complex structures, while increasing the power in sample 50/2/204 (Figure 5e) led to the formation of more beads (nucleation points) and shorter complex structures in comparison with 20/2/204.

All of these observations are in agreement with the structures morphogenesis of MAPPs on neat wafers as proposed by Brioude et al.¹² During the CW process, the intense excitation of both monomer and substrate results in a very high concentration of ions, radicals, and activated sites, leading to a high rate of deposition and homogeneous growth of the

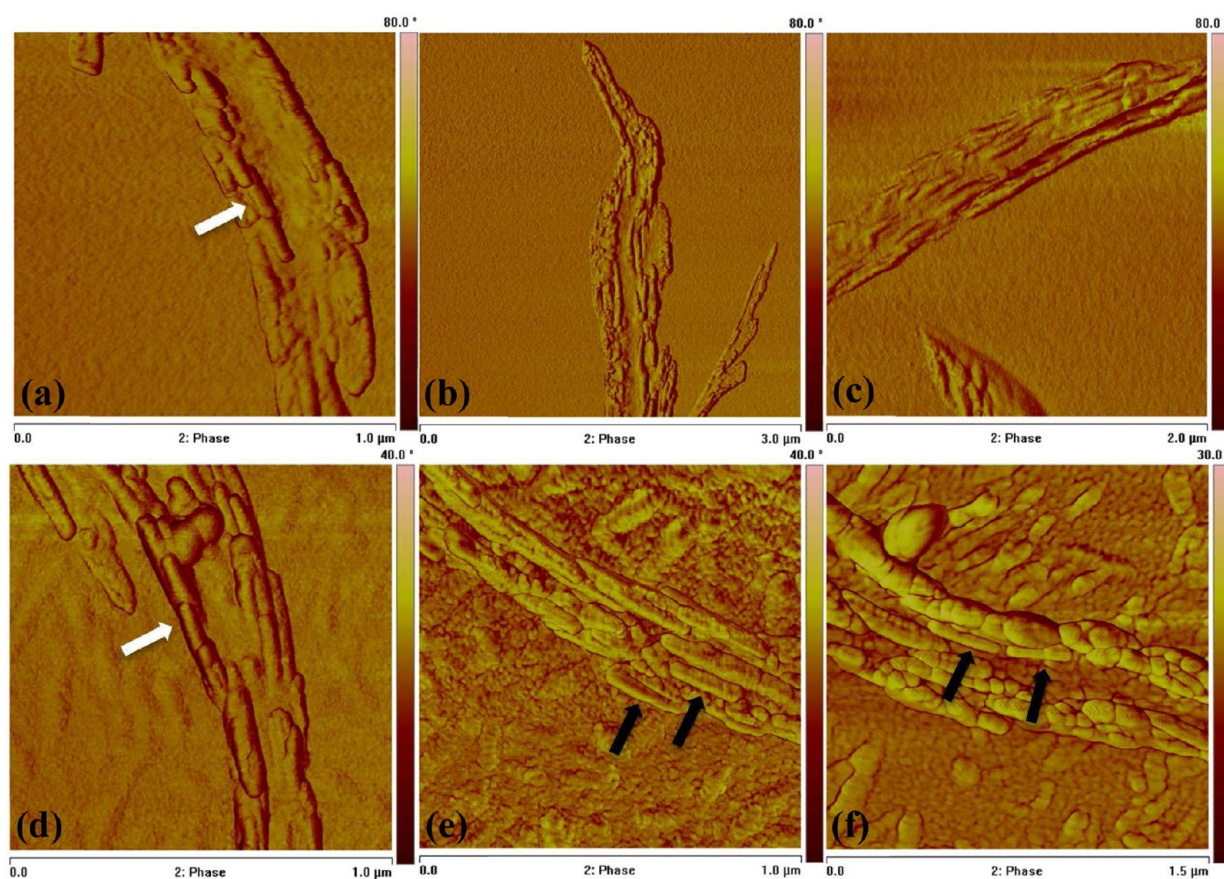


Figure 6. Phase AFM images of MAPP films deposited over (a–c) a silicon wafer substrate (without CNCs) and (d–f) silicon wafer substrates with homogeneously dispersed CNCs.

MAPP layer. In other words, since both ions and radicals are delivering mass for the film formation, the mechanism of plasma growth can be regarded as a hybrid ion/radical mode.^{52,53} The use of the pulsed process changes the mechanism of plasma growth; during the pulse-off time, only radicals participate to the plasma growth, which significantly reduces the presence of ions, shifting the growth mechanism to a purely radical growth mechanism. Therefore, for the pulsed process and a DC of 50%, a small decrease of the concentration of radicals and activated sites follows the decrease of the average power, and the presence of a short pulse-off time (ca. 2450 μ s) allows the diffusion of the radicals to the closest nucleation points, producing the beads. Further decrease of the DC results in lower average power but longer pulse-off time, that is, less activated sites but longer time for the radicals to migrate and react with the available nucleation sites. Expectedly, this leads to longer structures. The surface activated sites that result in the beads and afterward in the branched or needlelike structures are formed mainly during the very early stage of excitation due to positive ion bombardment. With the establishment of the equilibrium between the plasma phase and the surface, and the radical diffusion provided by the pulsed-off time, the reaction between radicals and nucleation sites is more favorable than the direct reaction with the surface. This results in the formation of beads and further development of branched/needlelike structures instead of creation of new nucleation sites (activation sites).¹³

The increase of the frequency from 204 to 1633 Hz greatly decreases the pulse-off time from 4800 to 600 μ s, resulting in shorter diffusion time and smaller structures. Finally, an

increase in the peak power causes an increase in the number of activated sites (more nucleation points) and consequently a higher amount of short structures and beads.

A close view over the structures developed by the MAPP on wafers with and without CNCs is shown in Figure 6. The analysis of the MAPP structures on the neat films shows that the structures are formed from locally heterogeneous MAPP growth. In some cases, the structures resemble aligned rods growing from the coating (white arrow in Figure 6a) or surface wrinkles (Figure 6b, c). For the samples deposited on the nanocellulosic surfaces, the presence of the CNCs below the coating is observed. The comparison between samples with and without CNCs does not reveal significant differences, and similarly aligned rods can be seen (white arrow in Figure 6d). However, some different rodlike-shaped formations in the structures are observed (black arrows in Figure 6d, e), suggesting the possibility that, during the growth of the structures, some CNCs are trapped and aligned parallel wise to the branches.

In general, no remarkable morphological difference could be observed by depositing the MAPP on a nanocellulosic surface composed of homogeneously dispersed CNCs or on the neat silicon wafer substrate.¹² The plasma conditions caused the same effects on MAPP morphology on the cellulosic surfaces as on the neat wafers. In contrast, the deposition of a MAPP on the micropatterned hydrophobic/hydrophilic wafer displaying CNC islands and areas with very low concentration of CNCs revealed a significant difference: the density of complex structures on the highly concentrated CNCs domain increased drastically (Figure 7). Such an increase in the number of

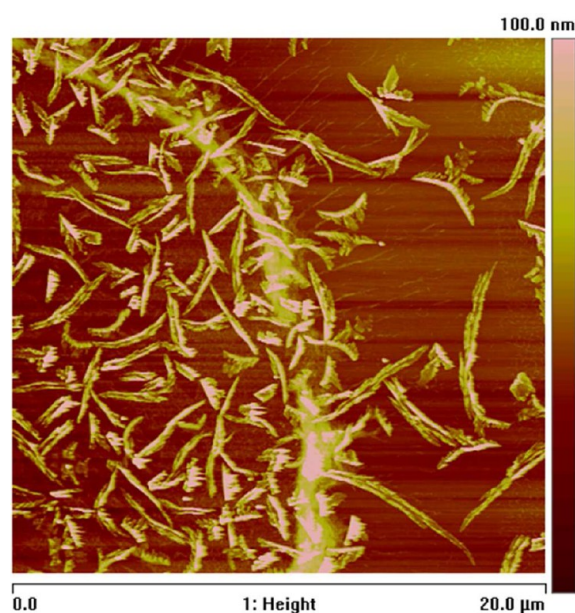


Figure 7. Height AFM images of MA plasma films deposited over a patterned substrate containing islands of high density of CNWs deposited at 20 W, 2%, 816 Hz, 20 min.

structures reflects the increase in the number of nucleation points, which in turn impacts the length of the structures due to impingement. In other words, more nucleation points for the same number of radicals results in more numerous, shorter structures. A similar observation arises when comparing samples 20/2/204 and 50/2/204 (Figure 5a and e, respectively), in which power increase has exactly the same effect.

The impact of differential CNC concentration can be quantified by calculating the structure surface fraction on the CNC islands and on the adjacent areas (low density of CNCs); the CNC islands registered an increase of structure surface fraction of $\sim 15\%$ compared to the CNC low-density area growing from approximately 20% to 35% (Table 2). On the

Table 2. Surface Fraction of Structures

	structure surface fraction
CNC low-density area	$19.5 \pm 3.6\%$
CNC island	$35.3 \pm 2.5\%$
homogeneously dispersed CNCs	$21.0 \pm 0.8\%$
silicon wafer without CNCs	$22.6\%^a$

^aRef 12.

other hand, there was no difference between this CNC low-density area, the neat silicon wafer, and the homogeneously dispersed CNCs. The similarities in structure surface fraction between the CNC low-density area on the micropatterned wafer and on the neat wafer were expected, since the chemistry and the surface energy of the substrate only affect the kinetics of growth in the very early stage of deposition during the plasma process.^{4,54} However, the similarity between the samples containing homogeneously dispersed CNCs and no CNCs (deposited on silicon wafer substrate) was surprising, since CNCs should act as nucleation sites, thus creating more structures or destabilizing the coating. The significant increase of the structure surface fraction deposited on the CNC islands demonstrates the ability of CNCs to act as a nucleation site but

only above a critical concentration. In other words, CNCs can catalyze the formation of complex structures in a MAPP but apparently only above a CNC concentration threshold.

CONCLUSION

The influence of CNCs on the morphology of MAPP films was investigated by comparing MAPP structure formation on wafers presenting a homogeneous and a heterogeneous/patterned distribution of CNCs. The homogeneous and heterogeneous nanocellulosic surfaces were produced by spin-coating a dilute CNC suspension on an etched wafer and on a hydrophobic/hydrophilic micropatterned wafer, respectively. AFM and optical microscopy evidenced that the etched, hydroxyl-rich silicon wafer substrate displayed a submonolayer of homogeneously distributed CNCs. However, spin-coating the CNC suspension on a hydrophobic silicon wafer patterned with circular hydrophilic microdomains of $86.9 \pm 4.9 \mu\text{m}$ resulted in the formation of CNC islands measuring $23.2 \pm 13.9 \mu\text{m}$ as a consequence of a wetting/dewetting and relaxation process. The deposition of the MAPP on both nanocellulosic surfaces revealed the same MAPP structuration process as previously evidenced on neat, cellulose-free wafers, with the existence of beads and complex branched and needlelike structures. Also, the impact of plasma conditions on the morphology of MAPPs on homogeneously distributed nanocellulosic surfaces resembled that on neat silicon wafers. No effect of CNC on MAPP morphogenesis could thus be revealed from this comparison, since the surface fractions of the structures were similar to values approximating 20%. In contrast, the heterogeneously distributed nanocellulosic surfaces exhibited a higher surface fraction of MAPP complex structures on the CNC island regions at around 35%, demonstrating that CNCs could act as nucleation points for complex structure formation in MAPPs. This further suggested that a CNC density threshold exists, above which such a nucleation effect is remarkable. This study therefore demonstrates that CNCs can be used to tailor-design topographical structuration in plasma polymerized maleic anhydride. Although no sign of destabilization could be observed on these films, some aging experiments are necessary in order to shed light on the role of CNCs on the MAPP nanostructured films stability. This aspect will be explored in further studies.

AUTHOR INFORMATION

Corresponding Author

*E-mail: marie-pierre.laborie@biomat.uni-freiburg.de.

Notes

The authors declare no competing financial interest.

ACKNOWLEDGMENTS

M.M.B. gratefully acknowledges the scholarship from Elisabeth and Barbara Grammel Foundation at the University of Freiburg and the COST Actions FP1006 – “Bringing new functions to wood through surface modification” and FP1205 – “Innovative applications of regenerated wood cellulose fibers” for the short term scientific missions support at the Université de Haute-Alsace, France. Special thanks also go to Tiago dos Santos for the sulfur content measurements of the CNCs.

REFERENCES

- (1) Samyn, P.; Airoudj, A.; Laborie, M.-P.; Mathew, A. P.; Roucoules, V. Plasma Deposition of Polymer Composite Films Incorporating Nanocellulose Whiskers. *Eur. Phys. J. Appl. Phys.* **2011**, *56*, 24015.
- (2) Friedrich, J. Mechanisms of Plasma Polymerization – Reviewed from a Chemical Point of View. *Plasma Processes Polym.* **2011**, *8*, 783–802.
- (3) Shi, F. F. Recent Advances in Polymer Thin Films Prepared by Plasma Polymerization: Synthesis, Structural Characterization, Properties and Applications. *Surf. Coat. Technol.* **1996**, *82*, 1–15.
- (4) Vasilev, K.; Michelmor, A.; Griesser, H. J.; Short, R. D. Substrate Influence on the Initial Growth Phase of Plasma-Deposited Polymer Films. *Chem. Commun.* **2009**, *24*, 3600–3602.
- (5) Cicala, G.; Milella, A.; Palumbo, F.; Rossini, F.; Favia, P.; D'Agostino, R. Nanostructure and Composition Control of Fluorocarbon Films from Modulated Tetrafluoroethylene Plasmas. *Macromolecules* **2002**, *35*, 8920–8922.
- (6) Cicala, G.; Milella, A.; Palumbo, F.; Favia, P.; D'Agostino, R. Morphological and Structural Study of Plasma Deposited Fluorocarbon Films at Different Thicknesses. *Diamond Relat. Mater.* **2003**, *12*, 2020–2025.
- (7) Favia, P.; Cicala, G.; Milella, A.; Palumbo, F.; Rossini, P.; D'Agostino, R. Deposition of Super-Hydrophobic Fluorocarbon Coatings in Modulated RF Glow Discharges. *Surf. Coat. Technol.* **2003**, *169–170*, 609–612.
- (8) Milella, A.; Palumbo, F.; Favia, P.; Cicala, G.; D'Agostino, R. Continuous and Modulated Deposition of Fluorocarbon Films from $c\text{-C}_4\text{F}_8$ Plasmas. *Plasma Processes Polym.* **2004**, *1*, 164–170.
- (9) Milella, A.; Palumbo, F.; Favia, P.; Cicala, G.; D'Agostino, R. Deposition Mechanism of Nanostructured Thin Films from Tetrafluoroethylene Glow Discharges. *Pure Appl. Chem.* **2005**, *77*, 399–414.
- (10) Milella, A.; Di Mundo, R.; Palumbo, F.; Favia, P.; Fracassi, F.; D'Agostino, R. Plasma Nanostructuring of Polymers: Different Routes to Superhydrophobicity. *Plasma Processes Polym.* **2009**, *6*, 460–466.
- (11) Di Mundo, R.; Gristina, R.; Sardella, E.; Intranuovo, F.; Nardulli, M.; Milella, A.; Palumbo, F.; D'Agostino, R.; Favia, P. Micro-/nanoscale Structuring of Cell-Culture Substrate with Fluorocarbon Plasmas. *Plasma Processes Polym.* **2010**, *7*, 212–223.
- (12) Brioude, M. M.; Laborie, M.-P.; Airoudj, A.; Haidara, H.; Roucoules, V. Controlling the Morphogenesis of Needle-like and Multibranched Structures in Maleic Anhydride Plasma Polymer Thin Films. *Plasma Processes Polym.* **2014**, *11*, 943–951.
- (13) Brioude, M. M.; Laborie, M.-P.; Haidara, H.; Roucoules, V. Understanding the Morphogenesis of Nanostructures in Maleic Anhydride Plasma Polymer Films via Growth Kinetics and Chemical Force Titration. *Plasma Processes Polym.* [Online early access, February 13, 2015]. DOI: 10.1002/ppap.201400224. Published Online: April 1, 2015. <http://onlinelibrary.wiley.com/doi/10.1002/ppap.201400224/full>
- (14) Evenson, S. A.; Fail, C. A.; Badyal, J. P. S. Controlled Monomolecular Functionalization and Adhesion of Solid Surfaces. *Chem. Mater.* **2000**, *12*, 3038–3043.
- (15) Hu, J. J.; Yin, C.; Mao, H. Q.; Tamada, K.; Knoll, W. G. Functionalization of Poly(ethylene terephthalate) Film by Pulsed Plasma Deposition of Maleic Anhydride. *Adv. Funct. Mater.* **2003**, *13*, 692–697.
- (16) Airoudj, A.; Schrodj, G.; Vallat, M.-F.; Fioux, P.; Roucoules, V. Influence of Plasma Duty Cycle during Plasma Polymerization in Adhesive Bonding. *Int. J. Adhes. Adhes.* **2011**, *31*, 498–506.
- (17) Pompe, T.; Zschoche, S.; Herold, N.; Salchert, K.; Gouzy, M.-F.; Sperling, C.; Werner, C. Maleic Anhydride Copolymers – A Versatile Platform for Molecular Biosurface Engineering. *Biomacromolecules* **2003**, *4*, 1072–1079.
- (18) Geissler, A.; Vallat, M.-F.; Fioux, P.; Thomann, J.-S.; Frisch, B.; Voegel, J.-C.; Hemmerle, J.; Schaaf, P.; Roucoules, V. Multifunctional Stretchable Plasma Polymer Modified PDMS Interface for Mechanically Responsive Materials. *Plasma Processes Polym.* **2010**, *7*, 64–77.
- (19) Nitschke, M.; Ricciardi, S.; Gramm, S.; Zschoche, S.; Herklotz, M.; Rivolo, P.; Werner, C. Surface Modification of Cell Culture Carriers: Routes to Anhydride Functionalization of Polystyrene. *Colloids Surf., B* **2012**, *90*, 41–47.
- (20) Bacharouche, J.; Badique, F.; Fahs, A.; Spanedda, M. V.; Geissler, A.; Malval, J.-P.; Vallat, M.-F.; Anselme, K.; Francius, G.; Frisch, B.; Hemmerlé, J.; Schaaf, P.; Roucoules, V. Biomimetic Cryptic Site Surface for Reversible Chemo- and Cyto-Mechanoresponsive Surfaces. *ACS Nano* **2013**, *7*, 3457–3465.
- (21) Kulaga, E.; Ploux, L.; Balan, L.; Schrodj, G.; Roucoules, V. Mechanically Responsive Antibacterial Plasma Polymer Coatings for Textile Biomaterials. *Plasma Processes Polym.* **2014**, *11*, 63–79.
- (22) Ryan, M. E.; Hynes, A. M.; Badyal, J. P. S. Pulsed Plasma Polymerization of Maleic Anhydride. *Chem. Mater.* **1996**, *8*, 37–42.
- (23) Schiller, S.; Hu, J.; Jenkins, A. T. A.; Timmons, R. B.; Sanchez-Estrada, F. S.; Knoll, W.; Foerch, R. Chemical Structure and Properties of Plasma-Polymerized Maleic Anhydride Films. *Chem. Mater.* **2002**, *14*, 235–242.
- (24) Siffer, F.; Ponche, A.; Fioux, P.; Schultz, J.; Roucoules, V. A Chemometric Investigation of the Effect of the Process Parameters during Maleic Anhydride Pulsed Plasma Polymerization. *Anal. Chim. Acta* **2005**, *539*, 289–299.
- (25) Mishra, G.; McArthur, S. L. Plasma Polymerization of Maleic Anhydride: Just What Are the Right Deposition Conditions? *Langmuir* **2010**, *26*, 9645–9658.
- (26) Paul, D. R.; Robeson, L. M. Polymer Nanotechnology: Nanocomposites. *Polymer* **2008**, *49*, 3187–3204.
- (27) Mukherjee, R.; Das, S.; Das, A.; Sharma, S. K.; Raychaudhuri, A. K.; Sharma, A. Stability and Dewetting of Metal Nanoparticle Filled Thin Polymer Films: Control of Instability Length Scale and Dynamics. *ACS Nano* **2010**, *4*, 3709–3724.
- (28) Kubo, M.; Takahashi, Y.; Fujii, T.; Liu, Y.; Sugioka, K.; Tsukada, T.; Minami, K.; Adschiri, T. Thermal Dewetting Behavior of Polystyrene Composite Thin Films with Organic-Modified Inorganic Nanoparticles. *Langmuir* **2014**, *30*, 8956–8964.
- (29) Revol, J. F.; Godbout, L.; Dong, X. M.; Gray, D. G. Chiral Nematic Suspensions of Cellulose Crystallites; Phase Separation and Magnetic Field Orientation. *Liq. Cryst.* **1994**, *16*, 127–134.
- (30) Eichhorn, S. J. Cellulose Nanowhiskers: Promising Materials for Advanced Applications. *Soft Matter* **2011**, *7*, 303–315.
- (31) Gray, D. G. Transcrystallization of Polypropylene at Cellulose Nanocrystal Surfaces. *Cellulose* **2008**, *15*, 297–301.
- (32) Han, J.; Zhu, Y.; Hu, J.; Luo, H.; Yeung, L.-Y.; Li, W.; Meng, Q.; Ye, Q.; Zhang, S.; Fan, Y. Morphology, Reversible Phase Crystallization, and Thermal Sensitive Shape Memory Effect of Cellulose Whisker/SMPU Nano-composites. *J. Appl. Polym. Sci.* **2012**, *123*, 749–762.
- (33) Pandey, J. K.; Lee, C. S.; Ahn, S. H. Preparation and Properties of Bio-nanoreinforced Composites from Biodegradable Polymer Matrix and Cellulose Whiskers. *J. Appl. Polym. Sci.* **2010**, *115*, 2493–2501.
- (34) Pei, A.; Zhou, Q.; Berglund, L. A. Functionalized Cellulose Nanocrystals as Biobased Nucleation Agents in Poly(L-lactide) (PLLA) – Crystallization and Mechanical Property Effects. *Compos. Sci. Technol.* **2010**, *70*, 815–821.
- (35) Siqueira, G.; Frascini, C.; Bras, J.; Dufresne, A.; Prud'homme, R.; Laborie, M.-P. Impact of the Nature and Shape of Cellulosic Nanoparticles on the Isothermal Crystallization Kinetics of Poly(ϵ -caprolactone). *Eur. Polym. J.* **2011**, *47*, 2216–2227.
- (36) Yu, H.; Qin, Z.; Zhou, Z. Cellulose Nanocrystals as Green Fillers to Improve Crystallization and Hydrophilic Property of Poly(3-hydroxybutyrate-co-3-hydroxyvalerate). *Prog. Nat. Sci.* **2011**, *21*, 478–484.
- (37) Samyn, P.; Matthew, A. P.; Airoudj, A.; Haidara, H.; Roucoules, V.; Laborie, M.-P. Metastable Patterning of Plasma Nanocomposite Films by Incorporating Cellulose Nanowhiskers. *Langmuir* **2012**, *22*, 1427–1438.

- (38) Kontturi, E.; Johansson, L.-S.; Kontturi, K. S.; Ahonen, P.; Thüne, P. C.; Laine, J. Cellulose Nanocrystal Submonolayer by Spin-Coating. *Langmuir* **2007**, *23*, 9674–9680.
- (39) Choi, W. M.; Park, O. O. Micropatterns of Colloidal Assembly on Chemically Patterned Surface. *Colloids Surf., A* **2006**, *277*, 131–135.
- (40) Bondeson, D.; Mathew, A.; Oksman, K. Optimization of the Isolation of Nanocrystals from Microcrystalline Cellulose by Acid Hydrolysis. *Cellulose* **2006**, *13*, 171–180.
- (41) Segal, L.; Creely, J. J.; Martin, A. E., Jr; Conrad, C. M. An Empirical Method for Estimating the Degree of Crystallinity of Native Cellulose Using the X-ray Diffractometer. *Text. Res. J.* **1959**, *29*, 786–794.
- (42) Dong, X. M.; Revol, J. F.; Gray, D. G. Effect of Microcrystallite Preparation Conditions on the Formation of Colloid Crystals of Cellulose. *Cellulose* **1998**, *5*, 19–32.
- (43) Abitbol, T.; Kloser, E.; Gray, D. G. Estimation of the Sulfur Content of Cellulose Nanocrystals Prepared by Sulfuric Acid Hydrolysis. *Cellulose* **2013**, *20*, 785–794.
- (44) Haidara, H.; Vonna, L.; Schultz, J. Kinetics and Thermodynamics of Surfactant Adsorption at Model Interfaces: Evidence of Structural Transitions in the Adsorbed Films. *Langmuir* **1996**, *12*, 3351–3355.
- (45) Hamad, W. Y.; Hu, T. Q. Structure-Process-Yield Interrelations in Nanocrystalline Cellulose Extraction. *Can. J. Chem. Eng.* **2010**, *88*, 392–402.
- (46) Kargarzadeh, H.; Ahmad, I.; Abdullah, I.; Dufresne, A.; Zainudin, S. Y.; Sheltami, R. M. Effect of Hydrolysis Conditions on the Morphology, Crystallinity, and Thermal Stability of Cellulose Nanocrystals Extracted from Kenaf Bast Fibers. *Cellulose* **2012**, *19*, 855–866.
- (47) Beck-Candanedo, S.; Roman, M.; Gray, D. G. Effect of Reaction Conditions on the Properties and Behavior of Wood Cellulose Nanocrystal Suspensions. *Biomacromolecules* **2005**, *6*, 1048–1054.
- (48) Sahu, N.; Parija, B.; Panigrahi, S. Fundamental Understanding and Modeling of Spin Coating Process: A Review. *Indian J. Phys.* **2009**, *83*, 493–502.
- (49) Mougin, K.; Haidara, H. Complex Pattern Formation in Drying Dispersions. *Langmuir* **2002**, *18*, 9566–9569.
- (50) Vancea, I.; Thiele, U.; Pauliac-Vaujour, E.; Stannard, A.; Martin, C. P.; Blunt, M. O.; Moriarty, P. J. Front Instabilities in Evaporatively Dewetting Nanofluids. *Phys. Rev. E* **2008**, *78*, 041601.
- (51) Crivoi, A.; Duan, F. Evaporation-Induced Branched Structures from Sessile Nanofluid Droplets. *J. Phys. Chem. C* **2013**, *117*, 7835–7843.
- (52) Michelmore, A.; Charles, C.; Boswell, R. W.; Short, R. D.; Whittle, J. D. Defining Plasma Polymerization: New Insight into What We Should Be Measuring. *ACS Appl. Mater. Interfaces* **2013**, *5*, 5387–5391.
- (53) Michelmore, A.; Steele, D. A.; Whittle, J. D.; Bradley, J. W.; Short, J. D. Nanoscale Deposition of Chemically Functionalized Films via Plasma Polymerization. *RSC Adv.* **2013**, *3*, 13540.
- (54) Vasilev, K.; Michelmore, A.; Martinek, P.; Chan, J.; Sah, V.; Griesser, H. J.; Short, R. D. Early Stages of Growth of Plasma Polymer Coatings Deposited from Nitrogen- and Oxygen-Containing Monomers. *Plasma Processes Polym.* **2010**, *7*, 824–835.